A Monte Carlo study of the influence of molecular flexibility on the phase diagram of a fused hard sphere model

Carl McBride and Carlos Vega[a)]
Departamento de Química Física, Facultad de Ciencias Químicas, Universidad Complutense de Madrid, Ciudad Universitaria 28040 Madrid, Spain

(Received 25 April 2002; accepted 5 September 2002)

A study of a rigid fully flexible fused hard sphere model [C. McBride, C. Vega, and L. G. MacDowell, Phys. Rev. E **64**, 011703 (2001)] is extended to the smectic and solid branches of the phase diagram. Computer simulations have been performed for a completely rigid model composed of 15 fused hard spheres $(15+0)$, a model of 15 fused hard spheres of which 2 monomers at one end of the model form a flexible tail $(13+2)$, and a model consisting of 15 fused hard spheres with 5 monomers forming a flexible tail $(10+5)$. For the $15+0$ model the phase sequence isotropic–nematic–smectic A–columnar is found on compression, and the sequence solid–smectic A–nematic–isotropic on expansion. For the $13+2$ model the phase sequence isotropic–nematic–smectic C is found on compression, and the sequence solid–smectic A–nematic–isotropic on expansion. For the $10+5$ model the phase sequence isotropic–glass is found on compression. The expansion runs displayed the phase sequence solid–smectic A–isotropic. The introduction of flexibility was seen to stabilize the smectic A phase at the expense of the nematic phase. © *2002 American Institute of Physics.* [DOI: 10.1063/1.1517604]

I. INTRODUCTION

In the field of soft condensed matter variations in the structure of the fluids constituent molecules can lead to dramatic changes in the collective behavior of the system. In the study of such systems computer simulation provides one with an invaluable tool. Computer simulations, either Monte Carlo or molecular dynamics,[1–3] allow one to describe and vary a model, and to view the resultant phase behavior.[4–9]

With the ever-growing power of computers, both in terms of memory capacity and with clock speed, it is now possible to simulate molecular systems that have an impressive degree of realism. As an example, recently Cook and Wilson have simulated a fully atomistic system that consists of 1000 molecules of the mesogen 4-(*trans*-4-*n*-pentylcyclohexyl)benzonitrile (PCH5).[10] However, due to the computational expense of such simulations, only a limited number of models may be examined and a limited region of the equation of state (EOS) explored.

In order to examine the influence of various aspects of a model it is often useful to simulate a simpler model. In recent years uniaxial rigid models have been the subject of extensive studies. The existence of nematic phases for hard ellipsoids[11,12] as well as smectic phases for hard spherocylinders[13,14] is well established. Another uniaxial model that has recently received attention is the linear tangent hard sphere model (LTHS). This model is composed of m tangent hard spheres in a rigid linear configuration. Simulations have been performed by Wilson,[15–17] Yethiraj and Fynewever,[18,19] Williamson and Jackson,[20] and Vega *et al.*[21] These simulations demonstrated the existence of nematic and smectic phases for the LTHS model. One of the motivations for such an active interest in tangent hard sphere systems is the presence of a theoretical description of these systems. In the 1980s, Wertheim proposed the thermodynamic perturbation theory for associating fluids (TPT1).[22–25] This theory, along with the extension of TPT1 to the limit of infinite association by Wertheim and by Chapman, Jackson, and Gubbins,[26,27] has made tangent hard sphere systems a popular choice of model for studies of the fluid phase. Taking the equation of state of the hard sphere monomer fluid as its only input the TPT1 theory provides an EOS for both rigid and flexible chains in the isotropic phase.[28,29] Recently, TPT1 has been extended to describe solids composed of tangent hard spheres,[30–32] providing excellent agreement with simulation results. An extension of TPT1 to the description of nematic and smectic phases would be of much interest.[33,34] One drawback of the LTHS model is that it is nonconvex, thus increasing the possibility of ''bottleneck'' problems during simulations, i.e., molecules becoming locked together in a metastable configuration.[20] However, if a model is built up of hard spheres that are permitted to overlap then this problem is reduced. One of the first simulations of a linear fused hard sphere model was that of Whittle and Masters.[35] The model used by Whittle and Masters consisted of eight hard spheres with a reduced bond length $L^*=L/\sigma=0.6$, where L is the bond length and σ the diameter of the hard sphere monomer. Compression of an isotropic fluid of the $m=8$ linear fused hard sphere model resulted in the formation of the nematic liquid crystal phase. More recently McBride *et al.*[36] and Tian *et al.*[37] have studied this model for $m=11$ and 15, again with $L^*=0.6$. These longer ''molecules'' formed both nematic and smectic phases.

Many real mesogenic compounds consist not only of a rigid section, but have flexible extremities.[4,5,38–40] An obvi-

a)Electronic mail: carlos@ender.quim.ucm.es

ous and interesting question is the effect of flexibility on the phase diagram. A study of a system composed of spherocylinders flanked by ideal flexible tails has been undertaken by Duijneveldt and Allen.[41] It was found that the addition of the flexible tails increases the range of stability of the smectic region at the expense of the nematic region. The linear hard sphere model provided a good candidate for the addition of flexible tails. This may be done by, for example, subjecting a number of ''monomers'' at the end of the model to Monte Carlo configurational bias moves. By comparing the phase diagram of a rigid model with m hard spheres to that of a model with m_r rigid spheres and m_f (such that $m=m_r+m_f$) flexible spheres the effect of flexible tails on the phase diagram may be studied. McBride *et al.*[36] have performed such a simulation. It was shown that the introduction of a flexible tail into the model shifted the isotropic–nematic transition to higher densities. In this study there was also evidence of smectic formation at higher densities. However, the aforementioned study concentrated on compression of isotropic fluids, with no reference to expansion from the solid phase. An advantage of expansion runs from the solid phase is to provide an indication of the relative stability of the mesophases with respect to freezing. A second feature in this publication, which was not implemented in Ref. 36, is the use of nonisotropic NpT moves. Isotropic NpT moves are adequate for the study of isotropic and nematic phases. However, the study of solid and smectic phases requires the implementation of nonisotropic volume changes.

The objective of this paper is to analyze in greater detail the phase diagram of a fused hard sphere model composed of 15 hard spheres monomers, having m_r rigid spheres and m_f spheres. Three cases will be considered, namely, $m_r=15,13,10$. In this way our goal is to establish clearly the effect of a flexible tail on the phase diagram. Nonisotropic NpT simulations were undertaken for the solid and smectic phases. Compression runs were initiated from an isotropic fluid, and expansion runs starting from the close packed solid. The close packed structure of those models can be related with the well-known close packed structure of hard dumbbells, which has been described in detail previously,[42] thus allowing one to establish solid conclusions as to the effect of a flexible tail on the phase diagram.

The structure of this paper is as follows: In Sec. II details of the Monte Carlo simulations are given; the model, and the starting configurations are presented in Sec. III. In Sec. IV the phase behavior is given. In Sec. V conclusions are drawn from this work.

II. MODEL AND COMPUTATIONAL TECHNIQUE

The rigid fully flexible fused hard sphere model (RFFFHS)[36] consists of a chain of m interaction sites; associated with each of these sites is a hard sphere potential.[43] Of these m interaction sites, m_r constitute a rigid section, and m_f a flexible tail. The model contains no expressions for bond bending or torsional terms, thus the flexible tail can access any configuration that is free from inter- and intramolecular overlap. Each of the interaction or ''monomer'' sites

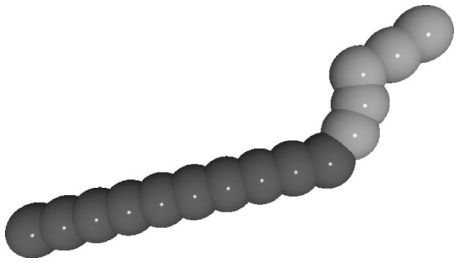

FIG. 1. Model used in this work. Snapshot of a $10+5$ ($m_r=10$, $m_f=5$) RFFFHS molecule in the gas phase. Sites corresponding to the rigid section and sites corresponding to the flexible section have been colored differently to aid the eye.

are of diameter $\sigma=1$. The bond length between consecutive monomers is $L^*=L/\sigma=0.6$. A snapshot of such a molecule is given in Fig. 1.

Flexibility was introduced into the tail by means of Monte Carlo configurational bias.[2] It should be noted that a bond length of $L^*=0.6$ restricts the center of a third sphere in a chain to a spherical cone of 67.1° from the axis of the cone. Temperature becomes a redundant variable for ''hard'' models; thus the properties of the system depend only on density. In this study three RFFFHS models were examined; a fully rigid model consisting of 15 monomers in a linear configuration (henceforth denoted $15+0$), a model of 13 monomers in a rigid configuration with a 2 monomer flexible tail ($13+2$ model), and a model of 10 monomers in a linear rigid configuration, with a tail built up of 5 flexible monomers ($10+5$ model).

Simulations were performed using Monte Carlo (MC) in the NpT ensemble.[2] The molecules were subjected to translational moves (45%) and rotational moves (45%). The remaining 10% of the MC moves were dedicated to the flexible tails using a configurational bias algorithm.[2] Nonisotropic volume moves were performed using the Rahman–Parinello technique.[44–47] A typical run consisted of 5×10^5 cycles for equilibration, followed by 3×10^5 cycles for production averages, one cycle being one trial move per molecule along with a trial volume move. During the simulations the nematic order parameter, S_2 (which is zero for an isotropic fluid and one for a perfectly aligned system), was continuously monitored (for details see Ref. 36). As well as the nematic order parameter snapshots of simulation configurations were also taken as a visual aid to phase identification.

The equation of state of a fluid can be described in terms of the compressibility factor, Z, where $Z=p/(\rho kT)$, with p being the pressure, $\rho=N/V$ the number density of the fluid (number of molecules per unit of volume), k the Boltzmann constant, and T the temperature. The compressibility factor can be expressed in terms of the packing fraction $y=\rho V_m$, where V_m is the molecular volume. The volume of a linear chain of m hard spheres of diameter σ and of bond length L is given by[48]

$$V_m=\frac{\pi}{6}\sigma^3\left[1+\frac{(m-1)}{2}\left(\frac{3L}{\sigma}-\left(\frac{L}{\sigma}\right)^3\right)\right]. \tag{1}$$

$V_m=6.329$ for the model used in this paper.

For isotropic state points obtained in this work a comparison is made to theoretical predictions provided by Wer-

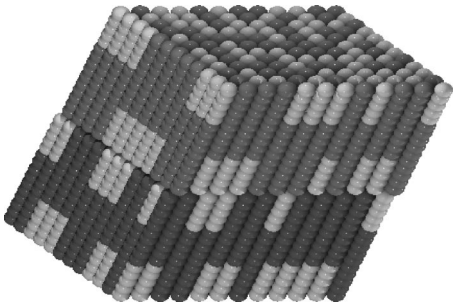

FIG. 2. Snapshot of the initial ''randomly flipped'' configuration for the 10+5 model (labeled the ''K1'' phase). Sites corresponding to the rigid section in each layer and sites corresponding to the flexible tails have been colored differently to aid the eye.

theim's thermodynamic perturbation theory (TPT1)[26,27] for tangent hard sphere chains. The compressibility factor for Wertheim's theory is given by

$$Z=\frac{p}{\rho kT}=m\frac{1+y+y^2-y^3}{(1-y)^3}-(m-1)\frac{1+y-\frac{y^2}{2}}{(1-y)\left(1-\frac{y}{2}\right)}, \tag{2}$$

where m is the number of tangent hard spheres forming the chain. Since TPT1 is designed for the tangent hard sphere model use has been made of an expression by Zhou *et al.*[49] which scales TPT1 for use with fused hard spheres. This mapping is given by an effective number of monomer units, m_{eff}. For $L^*\geqslant 0.5$ m_{eff} one has

$$m_{\mathrm{eff}}=\frac{(1+(m-1)L^*)^3}{(1+(m-1)L^*(3-L^{*2})/2)^2}. \tag{3}$$

For the model used in this study, having $L^*=0.6$, we have $m_{\mathrm{eff}}\approx 5.6843$.

III. INITIAL CONFIGURATIONS

A. Compression runs

Compression runs were started from a very low density α-face centered cubic structure.[1] All compression runs in this study consisted of 320 molecules. This number was arrived at by a $4\times4\times5$ lattice, with 4 molecules per unit cell. This initial structure has an order parameter of zero. During the equilibration section of the first low pressure run the crystalline structure of the initial configuration is lost. With the application of pressure an isotropic fluid condenses. The final configuration from a compression run was used as the initial configuration for a subsequent, higher pressure, run. Isotropic NpT Monte Carlo was used for the isotropic fluid and a change was made to nonisotropic NpT Monte Carlo simulations as soon as mesophases are formed.

B. Expansion runs

Expansion runs were started from a solid close packed structure (see Fig. 2). For more details on the construction of this solid structure see the hard diatomic CP1 packing in Refs. 42, 50. The 15+0 system consisted of four layers; each layer consisted of 9×9 molecules (324 molecules in total). For the 10+5 and the 13+2 systems the initial configurations consisted of two layers; each layer being a 12×12 lattice, thus the system contained 288 molecules in total.

For both the 10+5 and the 13+2 systems the molecules were ''randomly flipped.'' In the random flip structure each molecule is subjected to a random (50%) flip before it is added to the solid structure. This leads to a roughly even distribution of ''up'' and ''down'' molecules in the initial system. These molecules are placed ''head-to-foot,'' thus the flexible tails are in contact with the rigid sections.

For these structures the number density at close packing is $\rho_{\mathrm{cp}}=\rho\sigma^3\approx 0.1328$ ($y_{\mathrm{cp}}\approx 0.8403$). The solid structure depicted in Fig. 2 shall be labeled ''K1.'' In the K1 structure the molecules are tilted with respect to the layer normal.

TABLE I. Equation of state for compression runs for the 15+0 model from NpT MC simulations. $p^*=p\sigma^3/(kT)$, y is the volume fraction, and S_2 is the nematic order parameter. For the phases I=isotropic, N=nematic, and SmA is smectic A.

p^*	y	S_2	Phase
0.10	0.146	0.07	I
0.35	0.258	0.19	I
0.60	0.340	0.44	N
0.80	0.405	0.94	N
0.85	0.410	0.95	N
0.90	0.428	0.95	N
0.95	0.458	0.97	SmA
1.00	0.470	0.98	SmA
1.05	0.485	0.99	SmA
1.10	0.525	1.00	Columnar
1.15	0.533	1.00	Columnar
1.20	0.539	1.00	Columnar
1.25	0.545	1.00	Columnar
1.30	0.556	1.00	Columnar
1.35	0.559	1.00	Columnar
1.40	0.568	1.00	Columnar
1.45	0.570	1.00	Columnar
1.50	0.578	1.00	Columnar

IV. RESULTS

A. The 15+0 model

Three simulation runs were performed for the 15+0 model; a compression run, an expansion run from the solid structure analogous to that shown in Fig. 2, and a recompression run taken from a smectic A state point generated via the expansion route. The results for the compression runs for the 15+0 model are given in Table I. Results for the expansion runs are given in Table II. The results for the recompression are given in Table III. The equation of state is plotted in Fig. 3.

On expansion a solid/smectic A transition is observed at a packing fraction of $y\approx 0.55-0.56$. The smectic phase (Fig. 4) remains stable down to $y=0.40$ at which point a nematic phase forms. At $y=0.25$ the nematic phase becomes isotropic. In addition to the compression run and the expansion run a recompression run was undertaken. Starting from the end of the expansion run at $p^*=1.10$, in the smectic A phase, the

TABLE II. Equation of state for expansion run of the 15+0 model from NpT MC simulations. Notation as in Table I. The different phases have been labeled as in Table I, and K1 = solid structure as in Fig. 2.

p^*	y	S_2	Phase
100	0.835	1.00	K1
60	0.831	1.00	K1
40	0.827	1.00	K1
20	0.813	1.00	K1
15	0.804	1.00	K1
10	0.788	1.00	K1
8	0.776	1.00	K1
5	0.743	1.00	K1
3.0	0.678	1.00	K1
2.6	0.656	0.99	K1
2.4	0.643	0.99	K1
2.0	0.620	0.99	K1
1.8	0.607	0.99	K1
1.4	0.561	0.99	K1/SmA
1.35	0.553	0.99	K1/SmA
1.30	0.522	0.98	SmA
1.20	0.511	0.98	SmA
1.10	0.492	0.98	SmA
1.00	0.475	0.98	SmA
0.90	0.451	0.98	SmA
0.80	0.423	0.97	SmA
0.75	0.403	0.96	SmA/N
0.70	0.387	0.93	N
0.60	0.360	0.92	N
0.50	0.332	0.87	N
0.45	0.317	0.83	N
0.35	0.274	0.77	N
0.20	0.203	0.06	I

system was recompressed. On recompression a smectic A to solid transition was observed between the reduced pressure of $p^*=1.40$ and 1.55. The solid formed upon compression is of the type K1 (see Fig. 2). The molecular axes are tilted with respect to the normal of the layers. However, the solid formed upon compression present defects. All molecules within each layer point approximately in the same direction. The angle formed by the molecular axis with the normal of the layers is the same from one layer to another, so that all molecules of the system form a rather fixed angle with the normal of the layers. However, the direction of the molecular axis changes from one layer to another in a rather random way. For this reason, in the imperfect solid formed upon compression the molecular axis of all the molecules do not point in the same direction, and the order parameter (see Table III) remains locked and does not goes to one. For this reason the solid formed upon recompression is denoted as ''imperfect K1'' in Table III.

TABLE III. Equation of state for ''recompression'' runs for the 15+0 model from NpT MC simulations. Notation as in Table I. The different phases have been labeled as in Table I. The solid structure ''imperfect K1'' is defined in the text.

p^*	y	S_2	Phase
1.10	0.494	0.93	SmA
1.20	0.508	0.93	SmA
1.30	0.525	0.94	SmA
1.35	0.533	0.96	SmA
1.40	0.539	0.95	SmA
1.55	0.572	0.94	Imperfect K1
1.65	0.582	0.94	Imperfect K1
1.70	0.589	0.93	Imperfect K1
1.75	0.591	0.93	Imperfect K1
1.80	0.599	0.92	Imperfect K1
1.85	0.602	0.92	Imperfect K1
1.95	0.608	0.92	Imperfect K1
2.00	0.615	0.92	imperfect K1

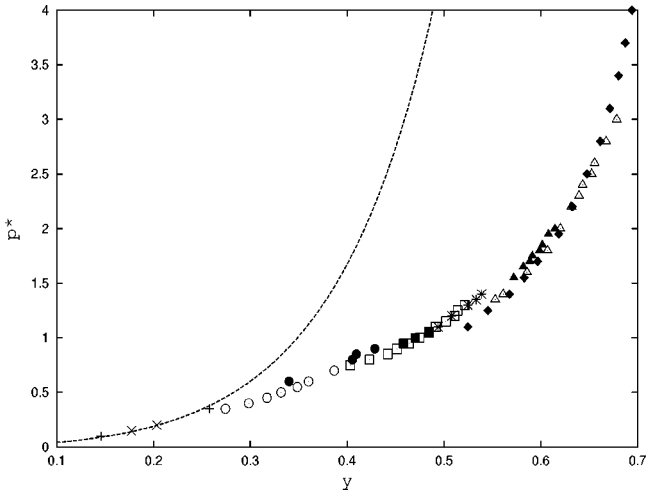

FIG. 3. The equation of state from the MC simulations for the 15+0 model. (+) isotropic (compression); (×) isotropic (expansion); (⊙) nematic (expansion); (●) nematic (compression); (*) SmA (recompression); (□) SmA (expansion); (■) SmA (compression)); (♦) columnar (compression); (▲) imperfect K1 solid (recompression); (△) K1 solid (expansion). The dotted curve represents the TPT1 EOS for the 15+0 RFFFHS model using the Zhou *et al.* (Ref. 49) correction. $p^*=p\sigma^3/(kT)$ and y is the packing fraction.

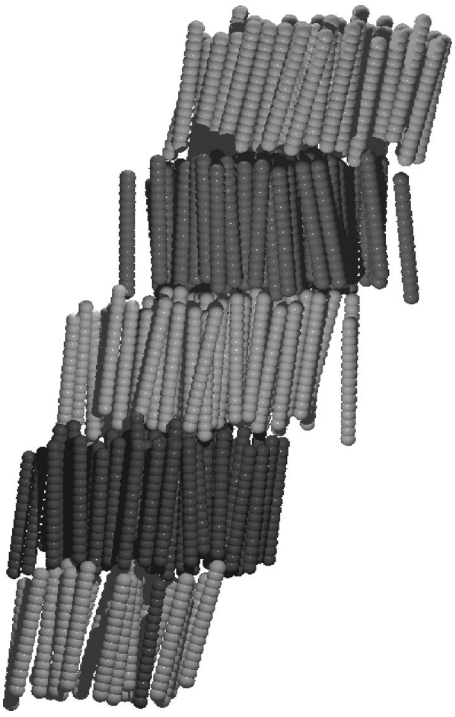

FIG. 4. Snapshot of the 15+0 model in the smectic A phase at a pressure of $p^*=1.00$. This configuration was generated during an expansion run.

TABLE IV. Equation of state for compression runs for the 13+2 model from NpT MC simulations. Notation as in Table I. SmC denotes a smectic C phase. The solid structure labeled as K2 is presented in Fig. 6. Segregation: the rigid chains and flexible tails form distinct domains. Tilt: tilt indicates that the molecular axes formed by the rigid part of the molecule are tilted with respect to the normal of the layers of the molecules.

p^*	y	S_2	Phase	Segregation	Tilt
0.1	0.149	0.03	I	No	
0.2	0.200	0.07	I	No	
0.3	0.236	0.08	I	No	
0.4	0.262	0.05	I	No	
0.5	0.285	0.10	I	No	
0.6	0.306	0.14	I	No	
0.7	0.338	0.49	N	No	
0.8	0.360	0.64	N	No	
0.9	0.382	0.87	N	No	
1.0	0.399	0.93	N	No	
1.2	0.435	0.95	N/SmC	No	
1.3	0.447	0.96	SmC	Yes	Yes
1.4	0.463	0.97	SmC	Yes	Yes
1.5	0.474	0.97	SmC	Yes	Yes
1.6	0.484	0.98	SmC	Yes	Yes
1.8	0.502	0.98	SmC	Yes	Yes
1.9	0.508	0.98	SmC/K2	Yes	Yes
2.0	0.519	0.98	SmC/K2	Yes	Yes
2.2	0.536	0.99	SmC/K2	Yes	Yes
2.3	0.554	0.99	K2	Yes	Yes
2.4	0.558	0.99	K2	Yes	Yes
2.6	0.572	0.99	K2	Yes	Yes
2.8	0.582	0.99	K2	Yes	Yes
3.0	0.591	0.99	K2	Yes	Yes

On compression a spontaneous ordering from the isotropic phase to the nematic phase is observed at a packing fraction of $y=0.30$. Once a nematic phase had formed the runs were then performed with anisotropic box scaling. At $y=0.458$ a nematic to smectic A transition is observed. As can be seen in Fig. 3 the equation of state of the smectic A phase obtained by compression is coincident with the smectic A phase obtained by expansion. At a packing fraction of 0.52 a columnar phase was encountered. In the columnar phase there is perfect long range hexagonal order in two dimensions with a fluid-like disorder of the centers of masses in the third dimension; the columnar has no layered structure. This is not to be confused with the smectic B structure, which has has a layered structure with short range hexagonal order within the layers (see Refs. 51, 52 for further details).

When compared to the K1 solid expansion run one sees that the columnar state points closely match the crystalline solid state points up to a packing fraction of $y=0.64$. It appears that the columnar phase and the solid phase have very similar free energies up to this packing fraction. It is possible that slight defects in the smectic system can be sufficient to induce a transition to the columnar phase rather than the layered solid. On further compression the columnar phase is unable to pack molecules as efficiently as a solid lattice. This is reflected in a lower density of the columnar structure with respect to a solid lattice at a given pressure. In view of this we suggest that the columnar phase is metastable with respect to the ordered solid. A small hysteresis loop is observed for the nematic to smectic transition with respect to compression/expansion indicating that the nematic to smectic transition is probably first order.

The isotropic state points for both compression and expansion runs lie very close to the TPT1 curve.

In summary the 15+0 system presents isotropic, nematic, smectic A, and solid phases. Each of the phases are found upon both expansion and compression. There appears to be little problem with accessibility between these phases.

B. The 13+2 model

In the 13+2 model the final two monomers at one extreme of the molecule are flexible. The configurational bias technique is used to sample the internal degrees of freedom of the flexible tail. For the 13+2 model, as with the 15+0 model, three simulation runs were performed; a compression run, an expansion run, and a recompression run. Simulation results for the compression runs are presented in Table IV. Compression of a low density isotropic configuration yields state points that are coincident with the TPT1 theoretical curve. At a pressure of $p^*=0.6$ the simulation results for the equation of state leave the TPT1 prediction and, at $p^* \approx 0.8$, an orientationally ordered nematic phase forms. Upon further compression, reaching a pressure of $p^* \approx 1.2$, a smectic C phase forms. Two layers of molecules form, each of the layers having a liquid-like structure. A snapshot of the smectic C phase at $p^*=1.4$ is presented in Fig. 5. It can be seen that the rigid and flexible segments appear to segregate. The smectic C phase obtained by compression is probably metastable with respect to freezing and is not believed to be a thermodynamically stable phase for this model. Upon further compression the rigid sections of the molecules freeze into an imperfect solid with translation order within the layers.

The expansion runs were initiated from a regular solid with a random flip of the molecules (see Fig. 2). In the initial configuration the layers consist of complete molecules; there is no separation of rigid and flexible units. On expansion, from $p^*=80$ to 20, no significant structural changes were observed. As the pressure was reduced to below $p^*=10$ important structural changes became apparent. Segregation is observed; the flexible tails form a fluid-like layer between the still solid-like rigid sections. For the purposes of labeling within this paper we shall name this structure ''K2.'' An illustrative snapshot of the K2 structure is presented in Fig. 6 for $p^*=2.8$. The direction of the tails is, on average, perpendicular to the layers formed by the rigid part of the molecules. In the snapshot the solid-like ordering of the rigid part and the liquid-like ordering of the flexible part is clearly visible. Simulation results for the expansion runs are given in Table V.

Upon further expansion, to a pressure of $p^* \approx 1.6$, a melting of the rigid sections is seen. This represents a transition from the K2 structure to the smectic A phase. A snapshot of the smectic A structure is presented in Fig. 7. It seems that, for the 13+2 model, melting is a two-stage process. In the first stage rigid and flexible parts segregate, with melting of the flexible tails. Then, as the pressure is further reduced, the rigid sections loose their close packed structure. This segregation of the rigid and flexible part of the molecules was observed both for compression and expansion runs.

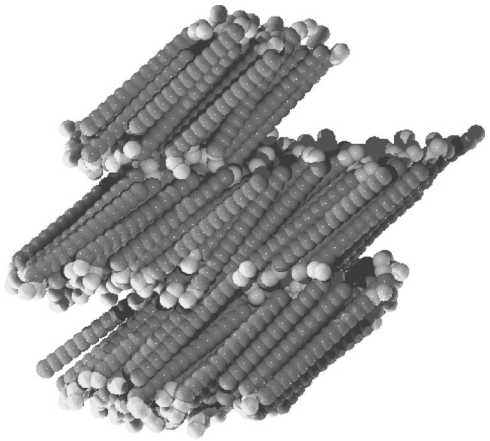

FIG. 5. Snapshot of the 13+2 model in the smectic C phase at a pressure of $p^*=1.40$ generated during a compression run.

Such segregation of rigid and flexible units was also found by McBride and Wilson[5] for a model whose rigid part consisted of a Gay–Berne site and whose flexible tails were alkyl chains. Although the chain lengths were asymmetric the Gay–Berne sites were found to group in to layers. However, it must be noted that the driving force in the McBride Wilson model for smectic formation is the strong value of the attractive forces between the Gay–Berne sites in the same layer. In the model described in this paper there are no attractive forces, and therefore the segregation of rigid and flexible sections in the smectic A phase is solely an entropic effect. This work shows that even in a purely repulsive model, entropic effects favor the separation of rigid and flexible sections.

Upon further expansion a smectic–nematic transition occurs at a pressure of $p^*=0.8$. The nematic phase transforms into an isotropic fluid at $p^*=0.5$.

A recompression run of the smectic A phase was performed. The recompression was initiated from the configuration generated at the end of the $p^*=1.2$ expansion run. A region of hysteresis was seen for the SmA–K2 transition at a pressure of $p^*\approx 2.2$. The simulation results are given in Table VI.

Figure 8 shows the equation of state obtained from these simulations. This figure summarizes the results obtained in this work for the 13+2 model. It also shows how the EOS obtained upon compression is not fully coincident with that obtained upon expansion. It is evident that the formation of defect free smectic or solid phases cannot be achieved using simulation runs of the length presented in this paper.

TABLE V. Equation of state for expansion runs for the 13+2 model from NpT MC simulations. Notation as in Tables I and IV.

p^*	y	S_2	Phase	Segregation	Tilt
80	0.833	1.00	K1	No	Yes
60	0.831	1.00	K1	No	Yes
40	0.826	1.00	K1	No	Yes
20	0.808	1.00	K1	No	Yes
10	0.753	1.00	K1	No	Yes
8	0.731	1.00	K1	No	Yes
6	0.684	1.00	K2	Yes	Yes
5	0.669	1.00	K2	Yes	Yes
4	0.638	1.00	K2	Yes	Yes
3	0.602	0.99	K2	Yes	Yes
2.8	0.596	0.99	K2	Yes	Yes
2.6	0.585	0.99	K2	Yes	Yes
2.4	0.577	0.99	K2	Yes	Yes
2.2	0.563	0.98	K2	Yes	Yes
2.0	0.543	0.99	K2	Yes	Yes
1.8	0.512	0.98	K2	Yes	Yes
1.6	0.498	0.97	SmA	Yes	No
1.4	0.473	0.97	SmA	Yes	No
1.2	0.452	0.95	SmA	Yes	No
1.0	0.419	0.94	SmA	Yes	No
0.8	0.366	0.83	N		No
0.6	0.318	0.66	N		No
0.5	0.282	0.13	I		No

In summary for the 13+2 model nematic, smectic C and solid phases are found upon compression. Upon expansion we found solid K1, solid K2, smectic A, nematic, and isotropic fluid. Notice, however, that the nematic range is significantly narrower than for the 15+0 model, whilst the range of stability smectic phase is wider.

C. The 10+5 model

In a similar manner to the 13+2 model, a compression run and expansion runs were performed as well as a recompression of a smectic phase.

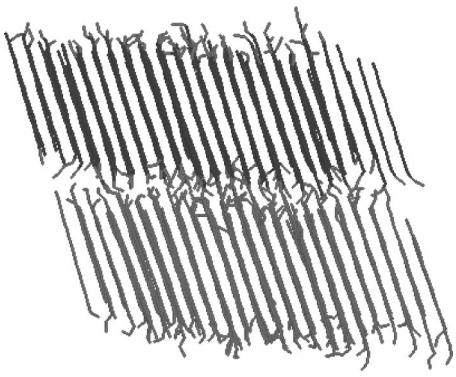

FIG. 6. Wire-frame snapshot of the 13+2 model in the solid ''K2'' phase at a pressure of $p^*=2.80$ generated during a expansion run.

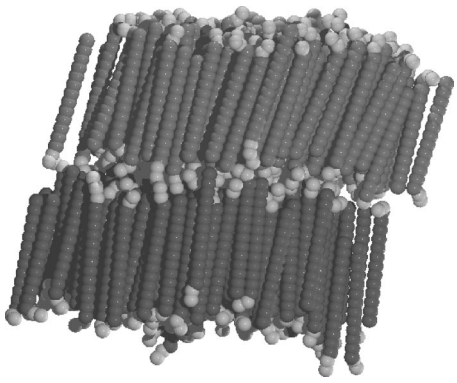

FIG. 7. Snapshot of the 13+2 model in the smectic A phase at a pressure of $p^*=1.60$ generated during an expansion run.

TABLE VI. Equation of state for recompression runs for the 13+2 model from the SmA phase. Notation as in Tables I and IV.

p^*	y	S_2	Phase	Segregation	Tilt
1.4	0.476	0.96	SmA	Yes	No
1.6	0.491	0.96	SmA	Yes	No
1.8	0.509	0.98	SmA	Yes	No
2.0	0.540	0.97	SmA/K2	Yes	No
2.2	0.557	0.98	K2	Yes	Yes
2.4	0.571	0.99	K2	Yes	Yes
2.6	0.585	0.98	K2	Yes	Yes
2.8	0.591	0.99	K2	Yes	Yes
3.0	0.602	0.98	K2	Yes	Yes
4.0	0.641	0.97	K2	Yes	Yes

On compression the isotropic fluid state points correspond with the TPT1 EOS. For $p^*>1.3$ ($y>0.38$) the EOS departs from the TPT1 curve. However, rather than finding a mesophasic state, a glass forms. If, as the expansion runs indicate, there is no nematic phase for this model then one should like to see an isotropic–smectic transition. Due to what is probably a substantial free energy barrier the simulations performed in this work were more than likely too short to see the spontaneous formation of a smectic phase. Given the degree of flexibility and the length of the flexible tails then such a ''rapid'' compression results in the glassy phase observed. This glassy state does not probably correspond to a true equilibrium configuration of the model.

The expansion runs were initiated from the K1 random flipped solid structure (Fig. 2). Results of the expansion run are presented in Table VII. In reducing the pressure from $p^*=80$ down to $p^*=5$ no significant structural changes are observed. On arriving at $p^*=4$, as with the 13+2 system, segregation of the flexible tails from the rigid section is seen. In a similar fashion to the 13+2 system the flexible tails form a fluid layer whilst the rigid sections are tilted and remain translationally ordered, i.e., the aforementioned ''K2'' structure. A snapshot of the system at $p^*=4$ is presented in Fig. 9.

When the pressure is reduced to below $p^*=2.4$ ($y<0.49$) the rigid layers lose their crystalline order and the system becomes smectic A. A snapshot of the system in the smectic A phase at a pressure of $p^*=1.8$ is presented in Fig. 10.

At a pressure of $p^*=1.6$ the smectic A phase starts to melt, and at a pressure $p^*=1.2$ the system is isotropic. No nematic phase is encountered. The range of pressures over which the the smectic A–isotropic transition occurs is most likely an indication of the long relaxation time associated with this transition. It is most probable that longer simulation runs would lead to a more precise location for this transition.

On recompression of the expansion run structure at $p^*=2.0$ the smectic A phase underwent a transition to the K2 structure at a pressure of $p^*=2.8$. For details of the simulation points see Table VIII. The EOS for this system is presented in Fig. 11.

In summary, upon compression isotropic and glassy states are obtained. Upon expansion the system passes through the phases, K1 solid, the K2 solid, the smectic A, and the isotropic fluid. The situation is similar to that presented for the 13+2 system, with the main difference being that no nematic phase is encountered, either on compression or on expansion. The addition of a flexible tail of five monomer units appears to suppress the nematic phase altogether. It is conceivable that an increase in the length of the flexible tail would completely suppress the formation of mesogenic phases.

In addition to the initial close packed random flip K1 structure studied so far, two other possible initial close packed configurations have been studied. These structures are the bilayer solid (presented in Fig. 12) and the ferroelectric. The ferroelectric structure is similar to the bilayer solid of Fig. 12; all of the molecules in one layer point in the same direction. The difference being is that each of the layers are the same as the layer above or below. Note that although the term ferroelectric is used there are no charges present and as such is not a true ferroelectric phase.

Expansion of the ferroelectric and the bilayer systems through the pressure range $p^*=80$ to 8 results in an EOS that is, to all intensive purposes, coincident with the EOS of the randomly flipped configuration. Without free energy calculations it is not possible to say which structure is the most stable in this pressure range. Only free energy calculations can establish which is the most stable phase (i.e., that with lower chemical potential for a certain pressure). However, the degeneracy entropy per particle associated with the random flip configuration is of the order of $kT\ln(2)$ (for a discussion of the degeneracy entropy in solid structures see Refs. 42, 53–55). This makes the random flip configuration the best candidate for the most stable of these three structures. Notice that other routes of determining the free energy such as thermodynamic integration or grand-canonical simulations cannot be used for determining the most stable solid phase. In fact thermodynamic integration (from low densities) cannot be used since we must cross first-order phase

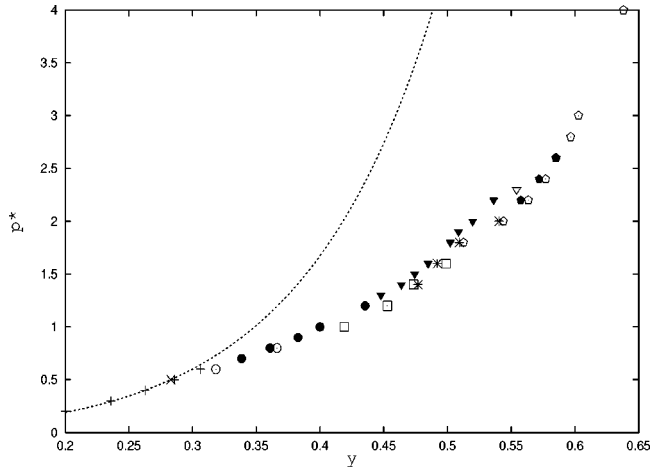

FIG. 8. The equation of state from the MC simulations for the 13+2 model. (+) isotropic (compression); (×) isotropic (expansion); (⊙) nematic (expansion); (●) nematic (compression); (*) SmA (recompression); (□) SmA (expansion); (▼) SmC (compression); black (pentagon) K2 (recompression); (pentagon) K2 (expansion); (▽) K2 (compression). The dotted curve represents the TPT1 EOS for the 15+0 RFFFHS model using the Zhou *et al.* (Ref. 49) correction.

TABLE VII. Equation of state for expansion runs for the 10+5 model from the random flip solid. Notation as in Tables I and IV.

p^*	y	S_2	Phase	Segregation	Tilt
80	0.833	1.00	K1	No	Yes
60	0.831	1.00	K1	No	Yes
40	0.826	1.00	K1	No	Yes
20	0.812	1.00	K1	No	Yes
10	0.759	1.00	K1	No	Yes
8.0	0.726	1.00	K1	No	Yes
6.0	0.655	1.00	K1	No	Yes
5.0	0.606	1.00	K1	No	Yes
4.0	0.563	0.97	K2	Yes	Yes
3.0	0.540	0.95	K2	Yes	Yes
2.8	0.531	0.96	K2	Yes	Yes
2.6	0.509	0.95	K2	Yes	Yes
2.4	0.499	0.94	K2/SmA	Yes	Yes
2.2	0.484	0.93	K2/SmA	Yes	Yes
2.0	0.472	0.91	SmA	Yes	No
1.8	0.455	0.90	SmA	Yes	No
1.6	0.438	0.90	SmA	Yes	No
1.4	0.408	0.72	SmA/I	Yes	No
1.2	0.372	0.34	I	No	
1.0	0.351	0.07	I	No	
0.8	0.327	0.10	I	No	
0.6	0.296	0.10	I	No	
0.5	0.279	0.05	I	No	

transitions and that invalidates the procedure, although for weak first-order phase transitions that could yield a first estimate.[56] Grand-canonical simulations present important technical difficulties since for the high dense phases considered in this work the probability of successfully inserting a particle (which in the case of hard bodies is related to the residual chemical potential) is almost zero.

At $p^*=6$ the flexible tails deviate from the initial linear molecular structure. The tails tend to become orientated parallel to the layer normal form by the rigid sections. The flexible tails become liquid-like whilst the rigid sections remain solid, thus resembling the K2 structure discussed previously.

In the pressure range $p^*=3$ to 1.4 the bilayer and ferroelectric systems form orientationally ordered phases. However, there are two clear indications that these structures are metastable. The first is the very poor equilibration of the system in this range of pressures. The second is provided by the fact that for a certain pressure, the density of the bilayer or ferroelectric structures are typically 3%–4% lower than those of the smectic A phase obtained upon expansion of the random flip configuration. This difference is larger than our statistical uncertainty in density for a certain pressure which is $\approx 0.8\%$.

At a pressure of $p^*<1.4$ both the ferroelectric and the bilayer structures melt into an isotropic fluid. These structures lack the degeneracy entropy associated with the random flip structure in the solid phase, and they yield a lower density for a certain pressure with respect to the random flip model in the mesophase. This allows one to effectively discard these structures as being stable solid phases for the 10+5 model.

An expansion run was also performed for a fourth structure. This structure is the inter-digitated structure (see Fig. 13). In this structure the molecules are displaced such that the flexible tails interlock. In generating this structure it is necessary for molecules in subsequent layers to be aligned with one another. Given this, it is not possible to generate the close packed structure and therefore one cannot arrive at the close packing fraction. Due to this, at very high pressures (between 8 and 80) the interdigitated phase yields for a given pressure a much lower density than the random-flip close packed structure. That is to say, that this is not the equilibrium structure at high pressures. For pressures below 6 the interdigitated structure yields identical phase behavior, both structurally and its EOS, to the random-flip structure, forming smectic A and isotropic phases.

V. CONCLUSION

In this paper the effect of flexible tails on the phase diagram of hard systems has been analyzed by means of Monte Carlo simulations. The model is formed by $m=15$ hard spheres with reduced bond length $L^*=0.6$. The first m_r monomers of the chain are arranged in a linear rigid configuration whereas the last m_f monomers are flexible. Three models were considered; the 15+0, the 13+2, and the 10+5 model. In our view the main conclusions that can be drawn from this work can be summarized as follows:

(1) Flexibility dramatically changes the appearance of the phase diagram of hard models; flexibility plays a major role in determining the appearance and location of the liquid crystal phases.

(2) Introducing flexibility in a model shifts the location of the isotropic–nematic transition to higher densities and

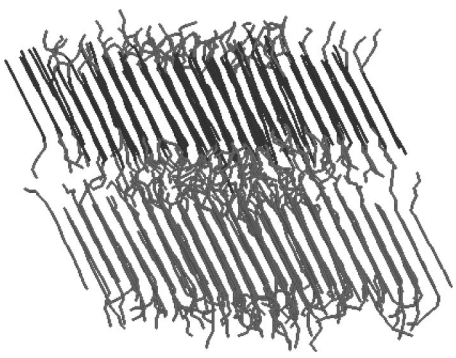

FIG. 9. Wire-frame snapshot of the 10+5 model in the K2 solid phase at a pressure of $p^*=4.00$ from an expansion run.

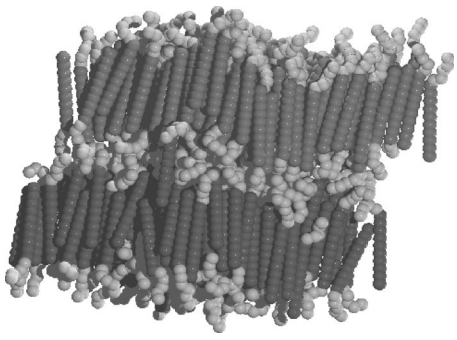

FIG. 10. Smectic A of the 10+5 model at a pressure of $p^*=1.80$.

TABLE VIII. The equation of state for the recompression runs of the 10 +5 model from the SmA phase. For phase definitions see Tables I and IV.

p^*	y	S_2	Phase	Segregation	Tilt
2.2	0.482	0.93	SmA	Yes	No
2.4	0.492	0.91	SmA	Yes	No
2.6	0.507	0.87	SmA/K2	Yes	No
2.8	0.525	0.88	K2	Yes	Yes
3.0	0.538	0.88	K2	Yes	Yes
4	0.579	0.91	K2	Yes	Yes
5	0.603	0.91	K2	Yes	Yes
6	0.623	0.91	K2	Yes	Yes
8	0.650	0.92	K2	Yes	Yes
10	0.669	0.92	K2	Yes	Yes

pressures. For the 10+5 model, no nematic phase was found either upon compression or upon expansion. The addition of flexible tails destabilizes the formation of nematic phases.

(3) The K1 random flip structure seems to be the most probable equilibrium structure at very high pressures for each of the models considered in this work. For the 13+2 and 10+5 models a new solid structure, the K2, is formed at high pressures. In the K2 structure there is a spontaneous segregation of the rigid and flexible sections; with solid ordering in the rigid layers and a fluid-like region formed by the flexible tails. The bilayer, ferroelectric, interdigitated structures are not considered to be equilibrium structures for this model.

(4) A smectic A phase is formed for the three models considered in this work, the 15+0, 13+2, and 10+5. In the smectic A phase, rigid and flexible units segregate. Since the models are composed of hard bodies this is merely an entropic effect. The typical range of stability of the smectic phase with respect to the solid does not depend much on the number of monomer units in the flexible tail. However, the stability of the smectic phase with respect to the isotropic fluid very much depends on the number of flexible monomer

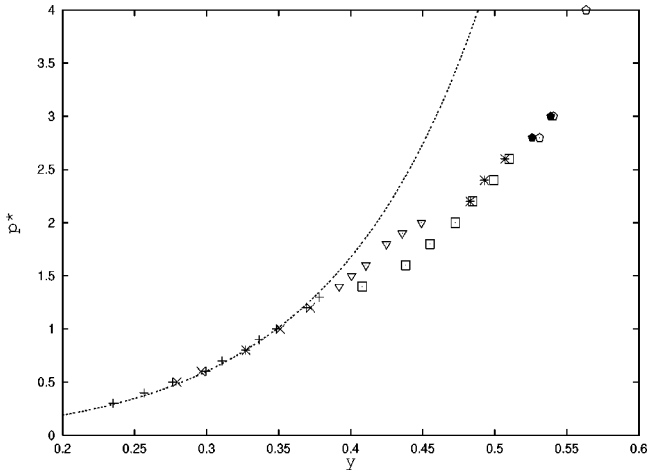

FIG. 11. The equation of state from the MC simulations for the 10+5 model. (+) isotropic (compression); (×) isotropic (expansion); (*) SmA (recompression); (□) SmA (expansion); (black pentagon) K2 (recompression); (pentagon) K2 (expansion); (▽) glass (compression). The dotted curve represents the TPT1 EOS for the 15+0 RFFFHS model using the Zhou *et al.* correction.

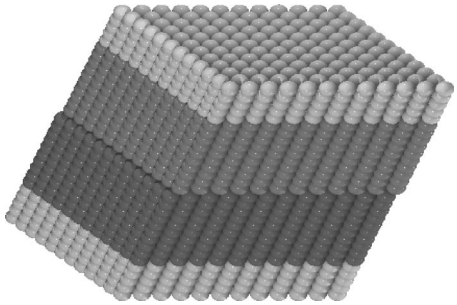

FIG. 12. Snapshot of the initial bilayer configuration for the 10+5 model. The layers are colored to aid visualization. The flexible tails are in light gray.

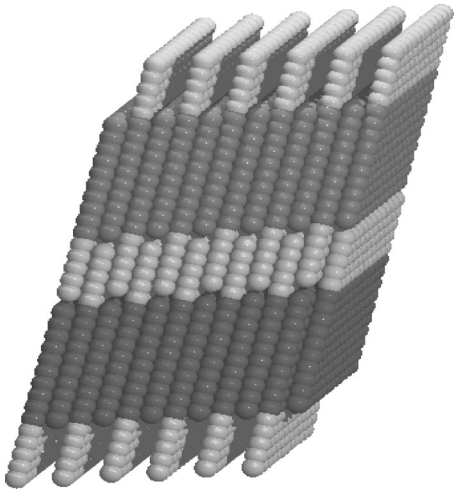

FIG. 13. Snapshot of the initial interdigitated configuration for the 10+5 model. The layers are colored to aid visualization. The flexible tails are in light gray.

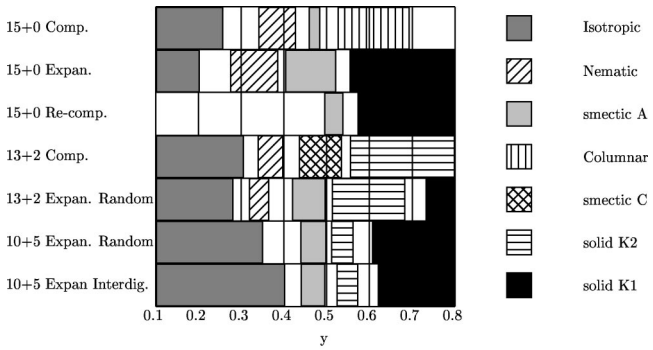

FIG. 14. Graphical representation of the phases found upon compression and expansion for the different models considered in this work.

units. For this reason it is likely that if the number of monomer units is too large (i.e., the $9+6$ or the $8+7$ models), the only transitions to be found would be the isotropic-crystal (K1 or K2) freezing, with no existence of mesophases in the phase diagram.

(5) A graphical summary of the results of this work can be found in Fig. 14.

Future areas of interest would be the addition of a dipole moment in one of the extremes of the molecule (in the rigid part), and/or incorporating biaxility in the model, by adding lateral rigid spheres in the rigid area of the molecule. That could bring the model of this work closer to the shape of real mesogen molecules.

ACKNOWLEDGMENTS

Financial support is due to Project No. BFM-2001-1420-CO2-01 of the Spanish DGICYT (Dirección General de Investigación Científica y Técnica). C.M. would like to acknowledge and thank the European Union FP5 Program for the award of a Marie Curie post-doctoral fellowship (No. HPMF-CT-1999-00163).

[1] M. P. Allen and D. J. Tildesley, *Computer Simulation of Liquids* (Oxford University Press, Oxford, 1987).
[2] D. Frenkel and B. Smit, *Understanding Molecular Simulation* (Academic, London, 1996).
[3] P. Pasini and C. Zannoni, *Advances in the Computer Simulations of Liquid Crystals* (Kluwer Academic, Dordrecht, 2001).
[4] C. McBride, M. R. Wilson, and J. A. K. Howard, Mol. Phys. **93**, 955 (1998).
[5] C. McBride and M. R. Wilson, Mol. Phys. **97**, 511 (1999).
[6] L. G. MacDowell, C. Vega, and E. Sanz, J. Chem. Phys. **115**, 6220 (2001).
[7] N. R. Kenkare, C. K. Hall, and S. A. Khan, J. Chem. Phys. **113**, 404 (2000).
[8] E. de Miguel, E. M. del Rio, J. T. Brown, and M. P. Allen, J. Chem. Phys. **105**, 4234 (1996).
[9] E. de Miguel, L. F. Rull, M. K. Chalam, and K. E. Gubbins, Mol. Phys. **74**, 405 (1991).
[10] M. J. Cook and M. R. Wilson, Mol. Cryst. Liq. Cryst. Sci. Technol., Sect. A **363**, 181 (2001).
[11] D. Frenkel and B. M. Mulder, Mol. Phys. **55**, 1171 (1985).
[12] P. J. Camp, C. P. Mason, and M. P. Allen, J. Chem. Phys. **105**, 2837 (1996).
[13] P. Bolhuis and D. Frenkel, J. Chem. Phys. **106**, 666 (1997).
[14] S. C. McGrother, D. C. Williamson, and G. Jackson, J. Chem. Phys. **104**, 6755 (1996).
[15] M. R. Wilson, Mol. Phys. **85**, 193 (1995).
[16] M. R. Wilson and M. P. Allen, Mol. Phys. **80**, 277 (1993).
[17] M. R. Wilson, Mol. Phys. **81**, 675 (1994).
[18] A. Yethiraj and H. Fynewever, Mol. Phys. **93**, 693 (1998).
[19] H. Fynewever and A. Yethiraj, J. Chem. Phys. **108**, 1636 (1998).
[20] D. C. Williamson and G. Jackson, J. Chem. Phys. **108**, 10294 (1998).
[21] C. Vega, C. McBride, and L. MacDowell, J. Chem. Phys. **115**, 4203 (2001).
[22] M. S. Wertheim, J. Stat. Phys. **35**, 19 (1984).
[23] M. S. Wertheim, J. Stat. Phys. **35**, 35 (1984).
[24] M. S. Wertheim, J. Stat. Phys. **42**, 459 (1986).
[25] M. S. Wertheim, J. Stat. Phys. **42**, 477 (1986).
[26] M. S. Wertheim, J. Chem. Phys. **87**, 7323 (1987).
[27] W. G. Chapman, G. Jackson, and K. E. Gubbins, Mol. Phys. **65**, 1 (1988).
[28] T. Boublik, C. Vega, and M. D. Pena, J. Chem. Phys. **93**, 730 (1990).
[29] Y. Zhou, S. W. Smith, and C. K. Hall, Mol. Phys. **86**, 1157 (1995).
[30] C. Vega and L. MacDowell, J. Chem. Phys. **114**, 10411 (2001).
[31] C. McBride and C. Vega, J. Chem. Phys. **116**, 1757 (2002).
[32] C. Vega and C. McBride, Phys. Rev. E **65**, 052501 (2002).
[33] K. M. Jaffer, S. B. Opps, and D. E. Sullivan, J. Chem. Phys. **110**, 11630 (1999).
[34] K. M. Jaffer, S. B. Opps, D. E. Sullivan, B. G. Nickel, and L. Mederos, J. Chem. Phys. **114**, 3314 (2001).
[35] M. Whittle and A. J. Masters, Mol. Phys. **72**, 247 (1991).
[36] C. McBride, C. Vega, and L. MacDowell, Phys. Rev. E **64**, 011703 (2001).
[37] P. Tian, D. Bedrov, G. D. Smith, and M. Glaser, J. Chem. Phys. **115**, 9055 (2001).
[38] J. W. Goodby and G. W. Gray, *Handbook of Liquid Crystals* (Wiley-VCH, Weinheim, 1998).
[39] F. Affouard, M. Kroger, and S. Hess, Phys. Rev. E **54**, 5178 (1996).
[40] G. L. Penna, D. Catalano, and C. A. Veracini, J. Chem. Phys. **105**, 7097 (1996).
[41] J. S. Duijneveldt and M. P. Allen, Mol. Phys. **92**, 855 (1997).
[42] C. Vega, E. P. A. Paras, and P. A. Monson, J. Chem. Phys. **96**, 9060 (1992).
[43] J. P. Hansen and I. R. McDonald, *Theory of Simple Liquids* (Academic, London, 1986).
[44] M. Parrinello and A. Rahman, Phys. Rev. Lett. **45**, 1196 (1980).
[45] M. Parrinello and A. Rahman, J. Chem. Phys. **76**, 2662 (1982).
[46] P. Najafabadi and S. Yip, Scr. Metall. **17**, 1199 (1983).
[47] S. Yashonath and C. N. R. Rao, Mol. Phys. **54**, 245 (1985).
[48] S. Varga and I. Szalai, Mol. Phys. **98**, 693 (2000).
[49] Y. Zhou, C. K. Hall, and G. Stell, J. Chem. Phys. **103**, 2688 (1995).
[50] C. Vega, E. P. A. Paras, and P. A. Monson, J. Chem. Phys. **97**, 8543 (1992).
[51] P. G. de Gennes and J. Prost, *The Physics of Liquid Crystals* (Clarendon, Oxford, 1995).
[52] D. Demus, J. Goodby, C. W. Gray, H.-W. Spiess, and V. Vill, *Physical Properties of Liquid Crystals* (Wiley VCH, Weinheim, 1999).
[53] K. W. Wojciechowski, D. Frenkel, and A. C. Brańka, Phys. Rev. Lett. **66**, 3168 (1991).
[54] K. W. Wojciechowski, A. C. Brańka, and D. Frenkel, Physica A **196**, 519 (1993).
[55] A. P. Malanoski and P. A. Monson, J. Chem. Phys. **107**, 6899 (1997).
[56] D. C. Williamson and F. del Rio, J. Chem. Phys. **109**, 4675 (1998).